Open Access

Advances in Environmental and Engineering Research

LIDSEN Publishing Inc.

Original Research

Integrated Assessment and Projection of Urban Expansion and Thermal Dynamics in Bangalore Using Multi-Temporal Landsat Data and Machine Learning Techniques

Rupesh Kumar Gupta *

Professor, Department of Continuing Education and Extension, Faculty of Social Sciences, University of Delhi, Delhi-110007, India; E-Mail: gisrs2004@gmail.com

* **Correspondence:** Rupesh Kumar Gupta; E-Mail: gisrs2004@gmail.com

Academic Editor: Amin Beiranvand Pour

Adv Environ Eng Res
2026, volume 7, issue 2
doi:10.21926/aeer.2602009

Received: February 12, 2026
Accepted: May 11, 2026
Published: May 19, 2026

Abstract

Rapid urbanization has remarkably altered land surface characteristics and thermal environments in Indian metropolitan cities, thereby increasing ecological pressure and urban heat risk. This study integrates assessments of land use and land cover (LULC) change and LST, and the UTFVI for Bangalore, India, using multi-temporal Landsat imagery and geospatial techniques, along with machine learning methods. LULC changes were studied and analyzed for 2000 and 2020, and a simulation to 2024 was performed, employing a Random Forest Classifier and a CA–ANN outline with the MOLUSCE model in QGIS. At the same time, seasonal LST and UTFVI patterns were studied for 2005, 2015, and 2025, and future thermal conditions were forecast for 2045 using Random Forest regression. The study's outcomes show remarkable growth in the urban region, with the built-up area increasing from 277.93 km^2 (12.64%) in 2000 to 501.89 km^2 (22.83%) in 2020, projected to be 666.19 km^2 (30.30%) by 2045. A sharp reduction in the areas of water bodies and vegetation cover accompanied this. The thermal analysis indicates a clear increase in warming during both summer and winter. There was also a consistent spreading pattern of moderate to high temperatures, ranging from 30-35°C and 35-40°C. According to the UTFVI, there is a shift in ecological thermal patterns, with a reduction in extreme "worst" levels of thermal stress zones and a considerable expansion of mid-levels. The study's results highlight the relationship between

land-use dynamics and urban thermal dynamics. Specifically highlighting the pressing need for climate-sensitive approaches in land-use planning, focus on the preservation of green and blue spaces, and the adoption of sustainable urban growth paths.

Keywords
Land use and land cover (LULC); land surface temperature (LST); urban thermal field variance index (UTFVI); remote sensing; machine learning; thermal environment; Google Earth Engine (GEE)

1. Introduction

One of the most important drivers of environmental change in the 21st century is rapid urbanization, which is altering surface energy balances and land systems while increasing the risks associated with climate change in cities worldwide. The expansion of the urban footprints causes significant changes in vegetation structure, hydrological processes, land use and land cover (LULC), plus the thermal properties of urban surfaces by replacing natural and semi-natural surfaces with impervious materials [1-4]. Aspects such as population growth, economic restructuring, and infrastructure expansion are occurring at a rate that frequently surpasses the capabilities of urban planning and environmental governance, making these changes especially noticeable in the Global South's fast-expanding cities [5-8].

The rise in air and surface temperatures is frequently reflected in the Urban Heat Island (UHI) effect. It is one of the most obvious environmental effects of urban growth. It is mainly because urban areas tend to have more heat-absorbing materials, less vegetation, less evapotranspiration, and more artificial heat emissions. Their land surface temperatures are often higher than those of nearby rural areas [9-11]. Air quality, ecosystems, energy use, public health, and human comfort are all impacted by rising land surface temperatures (LST) [12, 13]. Recent studies predict that urban thermal stress will increase further under future climate change scenarios, particularly in tropical and subtropical cities [14-17].

The urban areas of India serve as excellent examples of these difficulties. Major cities have experienced extensive LULC changes due to rapid urban growth driven by infrastructure development, economic liberalization, and demographic pressure. One obvious instance of this trend is Bangalore. The city has changed over the last few decades from a landscape of extensive vegetation and interconnected bodies of water to a dense, complex urban system in which built-up land predominates [18-22]. The farmland, wetlands, and green spaces are being converted into residential, commercial, and industrial zones due to increased pressure on land resources driven by the expansion of the information technology sector, rapid population growth, and peri-urban development [23-26].

Urban thermal environments are significantly shaped by LULC change. The Normalized Difference Vegetation Index (NDVI) is a vital instrument for measuring the cooling effects of vegetation, achieved through shading and evapotranspiration [27, 28]. Urban development-related impervious surfaces absorb and reradiate heat, thereby increasing LST values. This process is frequently measured with the Normalized Difference Built-up Index (NDBI) [29, 30]. The

fundamental role of land cover composition in regulating urban thermal behavior has been highlighted by numerous studies, which have demonstrated a robust negative association between NDVI and LST and positive associations between NDBI and LST [31-33].

The need to assess the ecological and environmental impacts of urban warming is increasingly recognized. It is not just about analyzing trends in absolute temperature. The Urban Thermal Field Variance Index (UTFVI) has emerged as a useful instrument for assessing ecological thermal stress by aggregating spatial variations in LST relative to the regional average [34, 35]. In addition to providing a useful framework for relating urban heat exposure to land cover types, environmental quality, and planning concerns, UTFVI helps identify regions with worsening thermal conditions. According to research using UTFVI in quickly expanding cities, ecological thermal stress is typically higher in areas with low vegetation and dense concrete [36, 37]. Monitoring and analyzing these intricate relationships have become much easier thanks to developments in geographic information systems (GIS) and satellite remote sensing. Long-term, spatially consistent evaluations of LULC dynamics, vegetation changes, and surface temperature patterns are made possible by the Landsat mission series' multispectral and thermal data [14, 18, 38]. Classification accuracy and predictive capabilities are further enhanced in a variety of urban environments by combining machine learning techniques with indices derived from remote sensing [35, 39]. Because of their resilience and ability to handle nonlinear relationships, Random Forest algorithms, in particular, show excellent performance in LULC classification and regression-based thermal variable prediction [8, 15, 40].

Spatial simulation models that integrate Cellular Automata (CA) and Artificial Neural Networks (ANN) are increasingly employed to predict future land-use patterns based on current development trends. These models, as implemented in platforms such as the Modules for Land Use Change Evaluation (MOLUSCE), incorporate neighborhood effects, transition probabilities, and complex interactions among land-use drivers, thereby enabling realistic scenario-based forecasts [41-44]. When combined with thermal indicators such as land surface temperature (LST) and the Urban Thermal Field Variance Index (UTFVI), CA–ANN frameworks offer a robust approach for evaluating the long-term effects of urban growth on thermal stress and environmental sustainability. While numerous studies have documented land LULC changes and urban heat dynamics in Bangalore, most have addressed these phenomena separately, focusing either on land-use transformation or surface temperature patterns over limited timeframes. Comprehensive assessments that integrate historical LULC changes, current thermal conditions, ecological thermal stress, and future projections within a unified framework remain limited. This deficiency constrains the capacity of planners and policymakers to anticipate emerging thermal risks and to formulate climate-responsive urban strategies grounded in empirical evidence.

This study contributes to the existing body of research by integrating land-use and land-cover dynamics, land-surface temperature patterns, and ecological thermal stress within a single analytical framework. Unlike previous studies that have largely examined these components in isolation, the present work combines multi-temporal analysis (2000-2025) with future projections (2045) using both Random Forest and CA–ANN modelling approaches. The inclusion of seasonal analysis further strengthens the understanding of temporal variability in urban thermal behavior. This integrated approach provides a more comprehensive assessment of urban expansion and its thermal implications, particularly in rapidly growing metropolitan environments.

2. Materials and Methods

2.1 Study Area

Bangalore, officially Bengaluru, is the capital of Karnataka. Bangalore is one of the country's fastest-growing metropolitan areas. Bangalore is located on the Deccan Plateau at an average elevation of about 920 meters above sea level. Geographically, Bangalore is positioned around 12°58′ N latitude and 77°34′ E longitude, covering an area of approximately 741 km^2. The current study has focused on the Bangalore Urban district, which is the principal area of urbanization and administrative activity of the city (Figure 1). Bangalore has experienced rapid demographic growth over the past two decades, with its population estimated at over 12 million. This expansion has been driven by economic development, particularly in the information technology sector, leading to increased pressure on land resources and urban infrastructure. Climatically, the region is characterized by approximately 900-1000 mm of average annual rainfall and temperatures typically ranging from 15°C to 35°C. These demographic and climatic conditions play a critical role in shaping land use transitions and urban thermal dynamics. The city experiences a tropical savanna climate with considerable seasonal changes throughout the year. In the summer, maximum temperatures are high, often exceeding 35°C during the day, whereas winters in Bangalore are quite pleasant, with temperatures often ranging between 15°C and 28°C. The city of Bangalore receives most of its rainfall during the southwest monsoon season, which is crucial for maintaining water levels and lush green landscapes; however, with increasing climatic changes and drastic alterations to landscapes because of human activities, the water and temperature levels of the place have been changing over the past few decades.

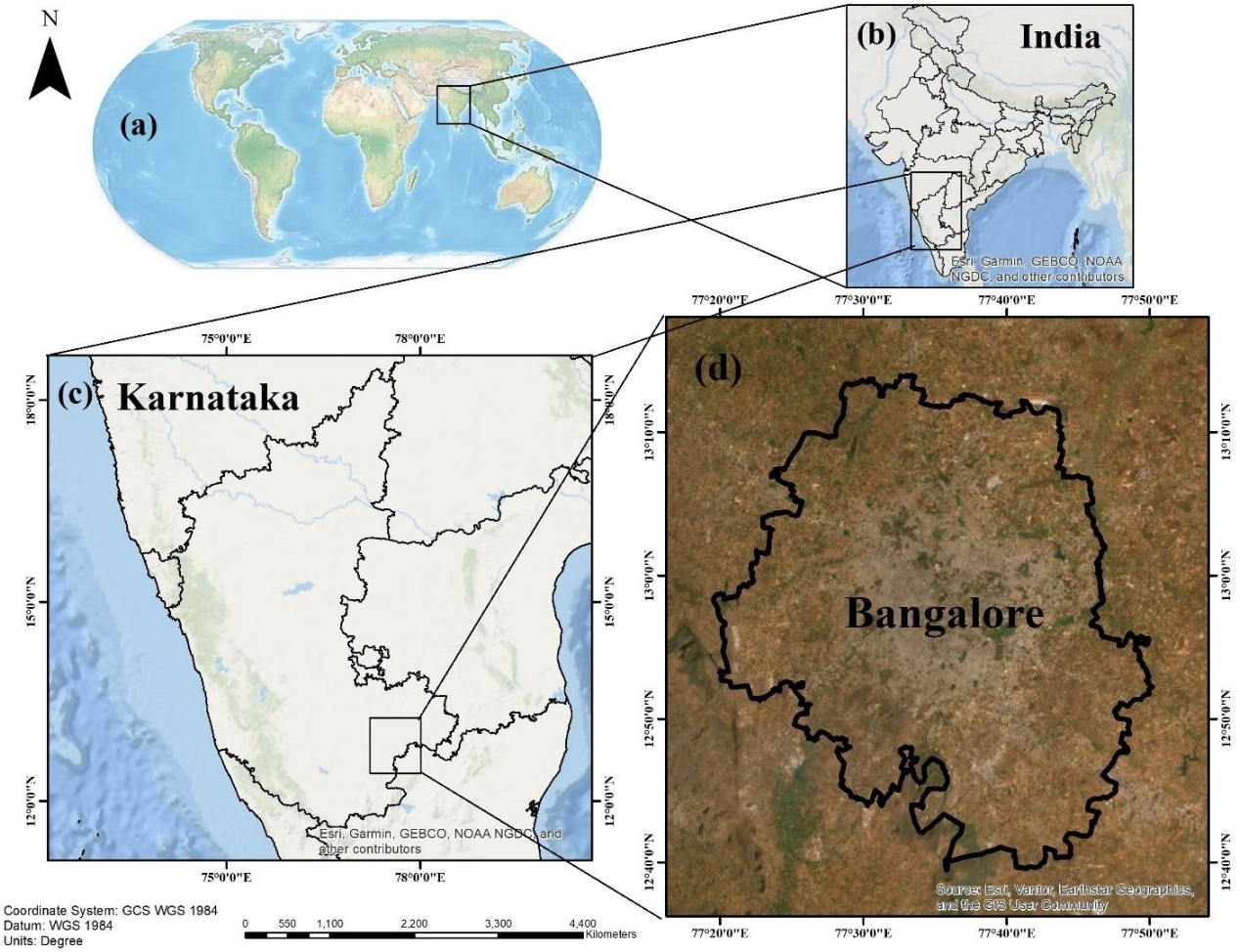

Figure 1 Study area showing (a) the location of the Indian subcontinent in the global context; (b) the location of India within the Indian subcontinent; (c) the location of Karnataka within India; and (d) the location of Bangalore.

2.2 Data Sources and Satellite Inputs

Multispectral and thermal datasets from the Landsat mission provide long-term, consistent, and freely available Earth observation data suitable for analyzing urban land and thermal dynamics. Landsat data are widely used in urban environmental and spatial research due to accurate calibration, adequate spatial resolution, and multi-decade temporal coverage. Landsat 7 Enhanced Thematic Mapper Plus (ETM+) imagery represents conditions in 2000. It establishes the historical baseline for LULC analysis. Landsat 8 Operational Land Imager and Thermal Infrared Sensor (OLI/TIRS) imagery was employed in 2020 to capture current land cover and thermal conditions. For thermal analysis and Urban Thermal Field Variance Index (UTFVI) assessment, additional datasets from Landsat 5 Thematic Mapper (TM), Landsat 8 OLI/TIRS, and Landsat 9 OLI/TIRS were used for 2005, 2015, and 2025 to support seasonal and multi-decadal land surface temperature (LST) evaluation. All optical and thermal datasets were obtained from the United States Geological Survey archive via Google Earth Engine. To address topographic effects on surface temperature, Shuttle Radar Topography Mission digital elevation data with a 30 m spatial resolution were incorporated into the thermal modelling and prediction stages. Table 1 and Table 2 provide an overview of the satellite datasets used for LULC and thermal analysis.

Table 1 Data Source and Acquisition Date used for LULC Classification of the study area.

Satellite	Acquisition Date	Resolution	Description
Landsat 7 ETM+	01/01/2000–31/12/2000	30 m	Landsat 7 Collection 2 Tier 1 and Real-Time data calibrated top-of-atmosphere (TOA) reflectance.
Landsat 8 OLI	01/01/2020–31/12/2020		

Table 2 Satellite Data Used to study LST and UTFVI.

Year	Satellite & Sensor	Bands Used	Spatial Resolution
2005	Landsat 5 TM	SR_B1–B7, ST_B6	30 m
2015	Landsat 8 OLI/TIRS	SR_B1–B7, ST_B10	30 m
2025	Landsat 9 OLI/TIRS	SR_B1–B7, ST_B10	30 m

2.3 Image Pre-processing and Harmonization

Google Earth Engine API was used for data acquisition, preprocessing, and initial analysis. The Bangalore Urban district boundary was prepared as a vector shapefile and uploaded to the platform to spatially constrain all processing steps. Satellite image collections were filtered by acquisition date, spatial extent, and cloud cover, with cloud contamination limited to <1% to reduce atmospheric interference.

For both LULC and thermal analysis, median composites were generated from filtered image collections to minimize noise from residual clouds, sensor artifacts, and short-term surface variability. These composites were clipped to the study area boundary to retain only relevant pixels. Surface reflectance products were used to confirm radiometric consistency across sensors because Landsat sensors differ in spectral response and radiometric characteristics. Physical harmonization was performed to standardize reflectance and brightness temperature values.

It ensured comparison across time periods and circumvented systematic bias in index calculation and temperature retrieval. The thermal analysis was generated from April to July for summer and from November to December for winter, which helps in seasonal compositing.

2.4 Land Use and Land Cover Classification

Supervised classification was used to generate LULC maps for Bangalore in 2000 and 2020. A total of six LULC classes were identified based on regional characteristics and planning significance, including built-up land, water bodies, dense vegetation, sparse vegetation, cropland, and barren land, shown in Table 3. Training samples were selected using visual interpretation of satellite imagery and ancillary reference data, informed by local knowledge of land cover patterns.

Table 3 Description of LULC Classification Outline.

LULC Type	Description
Built-up Land	Residential, Commercial, and Other Infrastructure
Water Body	Rivers, lakes, ponds, and dams
Dense Vegetation	All types of forest land
Sparse Vegetation	Parks, Green spaces, and wetlands
Crop Land	Agrarian Land, Ranch Land, Fallow Land
Barren land	All types of barren land

A buffer of 30 meters was applied to each training point to match the spatial resolution of Landsat imagery. The spectral reflectance values were extracted from these locations and used to train a Random Forest classifier. The configuration with 50 decision trees was used to balance classification accuracy and model generalization, with a special focus on reducing overfitting.

A trained classifier was applied separately to Landsat 7 ETM+ imagery from 2000 and to Landsat 8 OLI imagery from 2020. Classified outputs were visually inspected and color-coded for interpretation. The classification of built-up areas was carefully evaluated to minimize confusion with barren land, which often exhibits spectral characteristics similar to those of built-up areas in medium-resolution imagery. To address this, training samples were selected using high-resolution reference imagery and local knowledge of land cover patterns. In addition, post-classification validation was performed using Google Earth Pro imagery, where representative locations were visually verified to confirm the accuracy of built-up class identification. This step improved the reliability of class separation, particularly in transitional and heterogeneous urban areas. Overall accuracy, producer's accuracy, user's accuracy, and the Kappa coefficient were derived using the error matrix, and Classification accuracy was assessed. LULC maps, as the results, formed the basis for change detection and future simulation prediction.

2.5 Simulation of Future LULC Using MOLUSCE

The future land-use dynamics were simulated using the Modules for Land Use Change Evaluation (MOLUSCE) plugin in QGIS. The MOLUSCE framework uses Cellular Automata and Artificial Neural Network algorithms to model land-use transitions based on observed historical changes. Cellular Automata applies a Markovian postulation, in which it determines the future land-use pattern based on current conditions, and it is not overly dependent on historical arrangements.

The LULC maps for 2000 and 2020 were imported into QGIS and pre-processed to ensure consistent coordinate reference systems, spatial resolutions, and correct spatial extents. The classification schemes were standardized for both time periods. The transition probability matrix quantified conversion likelihoods over the 20-year period, which shows that the change detection analysis identified transitions between land-cover classes.

To capture nonlinear relationships between land-use change and the driving factors, ANN algorithms were used to estimate the transition potential in the study. To simulate land use conditions for 2045, the trained ANN model was applied. The results of the LULC projection provide a spatially clear representation of probable future development patterns under urban growth trends. The LULC simulation generated in this study represents a scenario-based projection derived from historical transition probabilities rather than a deterministic forecast. Due to limitations in

historical validation datasets and the scope of the present study, formal back-casting validation (e.g., simulating 2020 from 2000 and comparing with observed data) and advanced accuracy metrics such as Kappa, simulation, ROC/AUC, or Figure of Merit were not implemented. However, the CA–ANN model was calibrated using well-established transition rules and spatial drivers, and the results are intended to provide a plausible representation of future urban growth patterns under existing trends. Therefore, the projected LULC should be interpreted as an exploratory scenario that supports understanding of potential spatial dynamics rather than an exact prediction. This limitation has been acknowledged in the interpretation of results.

2.6 Derivation of Spectral Indices

The spectral indices were evaluated to assess vegetation health, calculate built-up density, and support thermal analysis. The Normalized Difference Vegetation Index (NDVI) was derived from the near-infrared and red bands to quantify vegetation greenness and concentration.

$$NDVI = \frac{NIR - RED}{NIR + RED} \tag{1}$$

High NDVI values indicate dense, healthy vegetation, whereas low NDVI values indicate sparse, stressed vegetation. The Normalized Difference Built-up Index (NDBI) was calculated using the shortwave and near-infrared bands to estimate the study area's impermeable surface area.

$$NDBI = \frac{SWIR1 - NIR}{SWIR1 + NIR} \tag{2}$$

Higher NDBI values correspond to built-up surfaces such as concrete and asphalt, which tend to retain heat.

2.7 Land Surface Temperature Retrieval

Land Surface Temperature was retrieved using an NDVI-based emissivity correction approach to ensure physically realistic temperature estimates. Fractional vegetation cover was first derived from NDVI:

$$FV = \left(\frac{NDVI - NDVI_{min}}{NDVI_{max} - NDVI_{min}}\right)^2 \tag{3}$$

Surface emissivity was then estimated as:

$$\varepsilon = 0.986 + 0.004 \cdot FV \tag{4}$$

Brightness temperature was corrected for surface emissivity using a standard Planck-based formulation:

$$LST = \frac{BT}{1 + \left(\frac{\lambda \cdot BT}{\rho}\right)\ln(\varepsilon)} - 273.15 \tag{5}$$

where *BT* is the at-sensor brightness temperature (in Kelvin), λ is the wavelength of emitted radiance (in meters; 10.8 μm for Landsat thermal bands), ε is the surface emissivity, and ρ is defined as:

$$\rho = \frac{h \cdot c}{k} \tag{6}$$

Here, h is Planck's constant (6.626×10^{-34} J·s), c is the speed of light (2.998×10^{8} m/s), and k is Boltzmann's constant (1.38×10^{-23} J/K). This formulation ensures physically consistent temperature retrieval from thermal infrared data. Table 4 represents classification of land surface temperature ranges and corresponding thermal exposure categories used for interpretation of heat stress levels.

Table 4 LST class intervals.

Class	Temperature (°C) Range	Interpretation
1	<30	Low thermal exposure
2	30-35	Moderate
3	35-40	High
4	40-45	Very high
5	>45	Extreme heat stress

2.8 Urban Thermal Field Variance Index

Urban thermal stress was assessed using the Urban Thermal Field Variance Index, which quantifies ecological thermal conditions relative to the regional mean temperature.

$$UTFVI = \frac{LST - LST_{mean}}{LST} \tag{7}$$

The UTFVI formulation used in this study follows a relative normalization approach in which local LST values scale temperature deviation. While alternative formulations normalize by the mean LST, the present form emphasizes pixel-level variability and enhances sensitivity to localized thermal conditions. This approach has been adopted in several studies of urban thermal environments to capture spatial heterogeneity in heat distribution better.

It is important to note that the choice of denominator may influence the magnitude of UTFVI values; however, it does not alter the relative spatial patterns of thermal stress. Therefore, the results are interpreted in terms of spatial distribution and comparative intensity rather than absolute index values [45, 46]. Higher UTFVI values indicate greater thermal stress and degraded ecological conditions. UTFVI values were classified into five ecological stress categories, as presented in Table 5.

Table 5 UTFVI classification categories.

UTFVI Range	UHI Presence	Ecological Meaning
<0.005	Weak	Good ecological condition
0.005-0.010	Middle	Normal
0.010-0.015	Strong	Bad
0.015-0.020	Stronger	Worse
>0.020	Strongest	Worst ecological condition

2.9 Machine Learning-Based Thermal Projection

The thermal conditions for the future were estimated using a Random Forest regression model trained on multi-temporal datasets from 2005, 2015, and 2025. Predictor variables included elevation, slope, geographic coordinates, NDVI, NDBI, NDWI, and temporal data. For future projections (2045), spectral indices such as NDVI, NDBI, and NDWI were derived from the simulated LULC map generated using the CA–ANN model. Each land-use class was associated with representative spectral characteristics based on historical relationships, enabling the generation of consistent predictor variables for the projected scenario. This approach ensures that the thermal model reflects dynamic land surface conditions rather than relying on static present-day inputs. The model was calibrated separately for summer and winter to account for seasonal variability. The projections were conducted for the year 2045, and the resulting LST and UTFVI maps were classified and analyzed to identify emerging thermal hotspots and regions of ecological pressure.

2.10 Ethical Statement

The present study relies completely on publicly available remote sensing and geospatial datasets obtained from open-access sources. No human participants, animals, humans, or identifiable personal or sensitive information were involved. Therefore, ethical approval from an institutional review board or ethics committee was not required. All data were utilized in accordance with the terms and conditions specified by the respective data providers, and the research adhered to established principles of research integrity and responsible data use.

3. Results and Discussions

3.1 Land Use and Land Cover Changes in Bangalore (2000-2020)

The classified LULC maps of Bangalore for 2000 and 2020 delineate six primary categories: Built-up Land, Water Bodies, Dense Vegetation, Sparse Vegetation, Cropland, and Barren Land. Table 6 summarizes the spatial distribution and areal proportions of these categories, and Figure 2 presents the corresponding LULC maps. The findings indicate notable landscape alteration over the two-decade period, primarily due to rapid urban expansion and subsequent land conversions.

Table 6 Area covered by various LULC classes and the percentage of cover for the years 2000 and 2020 in Bangalore.

Years	2000		2020	
Classes	**Area (Km^2)**	**Percentage**	**Area (Km^2)**	**Percentage**
Built-Up Land	277.93	12.64	501.89	22.83
Water Body	48.15	2.19	18.43	0.83
Dense Vegetation	560.42	25.49	484.37	22.03
Sparse Vegetation	622.37	28.31	147.15	6.69
Crop Land	677.02	30.79	892.94	40.62
Barren Land	12.23	0.55	153.32	6.97

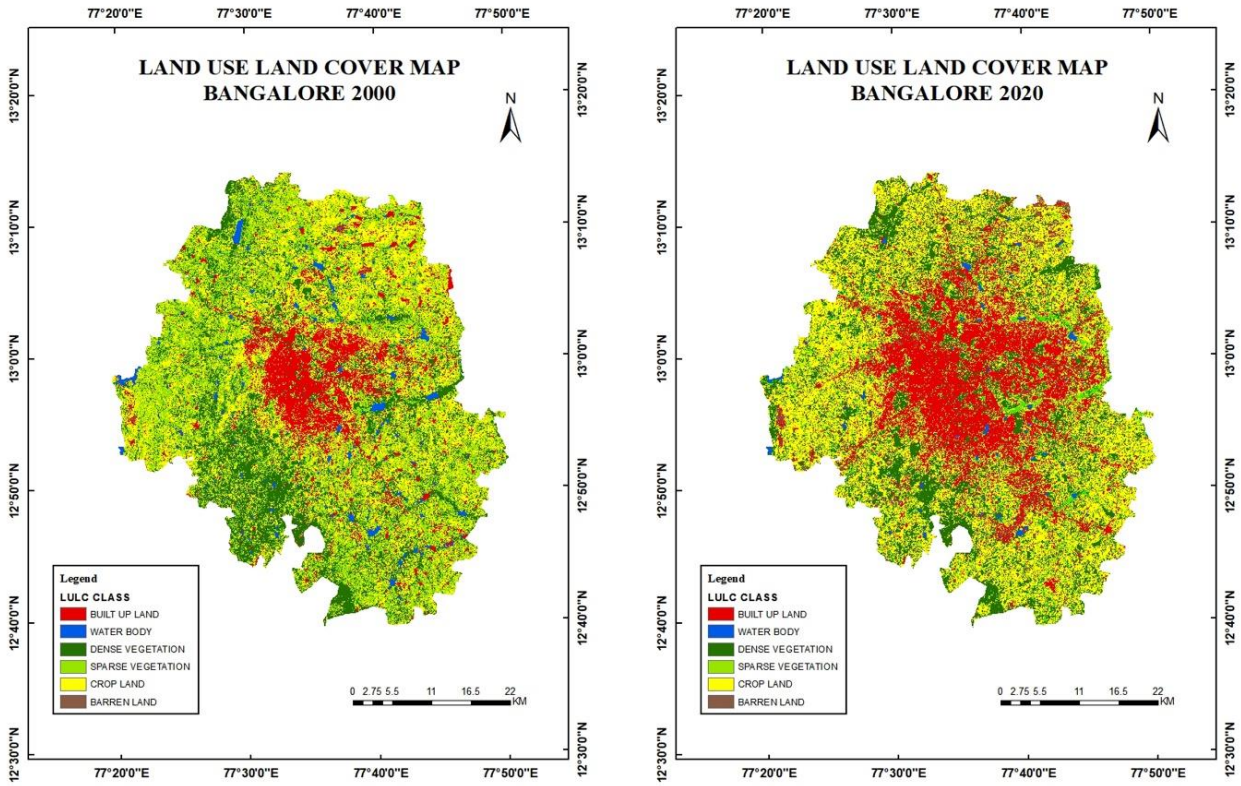

Figure 2 LULC Map of the study area in Bangalore for 2000 and 2020**.**

The built-up land area exhibited the largest increase, expanding from 277.93 sq. km (12.64%) in 2000 to 501.89 sq. km (22.83%) in 2020. As per the results, this noticeable growth is attributable to rapid urbanization and population growth. This situation heightened demand for residential, commercial, and industrial infrastructure. Apparently, the water bodies declined markedly, from 48.15 sq. km (2.19%) to 18.43 sq. km (0.83%). This constitutes a loss exceeding 60%. The reduction of lakes and wetlands suggests extensive encroachment and land filling, leading to hydrological alteration with significant consequences for groundwater recharge, flood mitigation, and the regulation of urban thermal dynamics.

The vegetation cover also decreased significantly during the study period. The area of dense vegetation decreased from 560.42 sq. km (25.49%) to 484.37 sq. km (22.04%). This result indicates a gradual reduction of established urban green spaces. Even more dramatic was the loss of sparse

vegetation, which declined from 622.37 sq. km (28.31%) to 147.15 sq. km (6.69%). This change highlights the large-scale conversion of open and semi-natural areas into built-up and agricultural land. This results in habitat fragmentation and loss of ecosystem services. Cropland expanded significantly from 677.02 sq. km (30.80%) to 892.94 sq. km (40.62%). This result reflects increased food demand associated with urban population growth. However, this expansion contributes to food security. It also increases pressure on water resources and soil health. The area under barren land rises significantly from 12.23 sq. km (0.56%) to 153.32 sq. km (6.98%). This indicates land degradation, abandonment of depleted agricultural fields, and regions affected by construction and environmental stress. Collectively, the observed LULC changes demonstrate a pronounced shift toward human-dominated land uses, resulting in substantial reductions in water bodies and vegetation. While the projected LULC patterns provide useful insights into potential future urban expansion, they should be interpreted with caution. The simulation reflects continuation of observed historical trends and does not explicitly account for future policy interventions, planning regulations, or unexpected socio-economic changes. As such, the results are best understood as indicative scenarios rather than precise forecasts, highlighting areas that may experience significant transformation under current development trajectories.

3.1.1 Accuracy Assessment of LULC Classification

The reliability of the LULC classification for Bangalore Urban was evaluated using a GIS-based Accuracy Assessment Tool. A total of 100 validation points were randomly distributed across the study area to assess classification accuracy. While a larger sample size may further improve statistical robustness, the selected sample provided a representative distribution across all land use classes and enabled reliable estimation of classification performance. The classified LULC outputs were validated using high-resolution Google Earth Pro imagery as reference data. Confusion matrices were constructed, and standard accuracy metrics, including overall accuracy, producer's accuracy, and user's accuracy, were calculated. The assessment yielded an overall classification accuracy of 89 percent for 2020, demonstrating strong agreement between the classified map and the reference data. This high level of accuracy indicates that classification errors were minimized. To further strengthen validation, high-resolution Google Earth Pro imagery served as a proxy for ground truthing, enabling visual verification of land cover classes at multiple locations, particularly for well-defined categories such as built-up areas and water bodies. Although the number of validation samples is moderate relative to the study area, care was taken to ensure spatial representation across all land-use categories. Future studies may incorporate stratified random sampling with a larger number of validation points to further enhance classification reliability. Despite this limitation, the achieved accuracy indicates strong agreement between classified outputs and reference data. Representative comparisons were made between classified outputs and actual ground conditions. Although field-based ground photographs for 2000 were unavailable, integrating multi-temporal Google Earth imagery enhanced the transparency, credibility, and robustness of the classification results.

3.2 Seasonal Variations in Land Surface Temperature in Bangalore (2005-2025)

The Seasonal analysis of Urban Land Surface Temperature (LST) across Bangalore indicates a clear intensification of urban thermal conditions between 2005 and 2025, marked by pronounced shifts in both the spatial extent and dominance of temperature classes (Table 7; Figure 3 and Figure 4). The observed patterns reflect the combined effects of rapid urban expansion, declining vegetation, and increasing surface imperviousness with distinct seasonal results in summer and winter. Bangalore's thermal landscape featured relatively cooler surface conditions in summer 2005. Areas with temperatures below 30°C covered 401.95 sq. km, while the 30-35°C class dominated the city, occupying 1,407.30 sq. km. Moderately high temperatures between 35-40°C were limited to 384.51 sq. km, and extreme heat conditions were almost negligible, with areas above 40°C together accounting for less than 2.5 sq. km. This distribution reflects a landscape that still retains considerable thermal buffering capacity due to vegetation, open spaces, and surface moisture.

Table 7 Summarized Table of LST for Summer and Winter Seasons in 2005, 2015, 2025.

LST (in °C)	Area (in sq. km)			Net Change (in sq. km)			Change in Percentage		
	2005	2015	2025	2005-15	2015-25	2005-25	2005-15	2015-25	2005-25
Summer Season									
Less than 30	401.95	56.49	174.81	-345.46	+118.32	-227.14	-85.95	+209.45	-56.51
30-35	1407.30	1414.88	1795.00	+7.58	+380.12	+387.70	+0.54	+26.87	+27.55
35-40	384.51	719.66	225.57	+335.15	-494.09	-158.94	+87.16	-68.66	-41.34
40-45	2.13	5.01	0.71	+2.88	-4.30	-1.42	+135.21	-85.83	-66.67
Above 45	0.23	0.07	0.03	-0.16	-0.04	-0.20	-69.57	-57.14	-86.96
Winter Season									
Less than 30	404.43	184.34	174.81	-220.09	-9.53	-229.62	-54.42	-5.17	-56.78
30-35	1333.40	1828.48	1795.00	+495.08	-33.48	+461.60	+37.13	-1.83	+34.62
35-40	454.99	182.58	225.57	-272.41	+42.99	-229.42	-59.87	+23.55	-50.42
40-45	3.07	0.68	0.71	-2.39	+0.03	-2.36	-77.85	+4.41	-76.87
Above 45	0.23	0.03	0.03	-0.20	0.00	-0.20	-86.96	0.00	-86.96

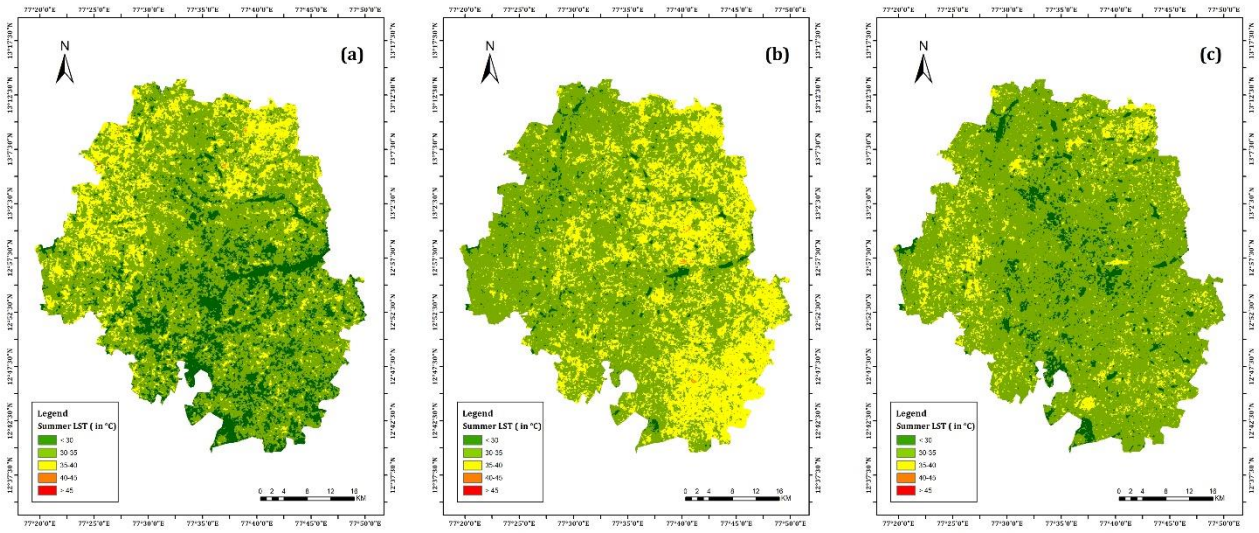

Figure 3 Summer LST distribution in the study area: (a) 2005, (b) 2015, and (c) 2025.

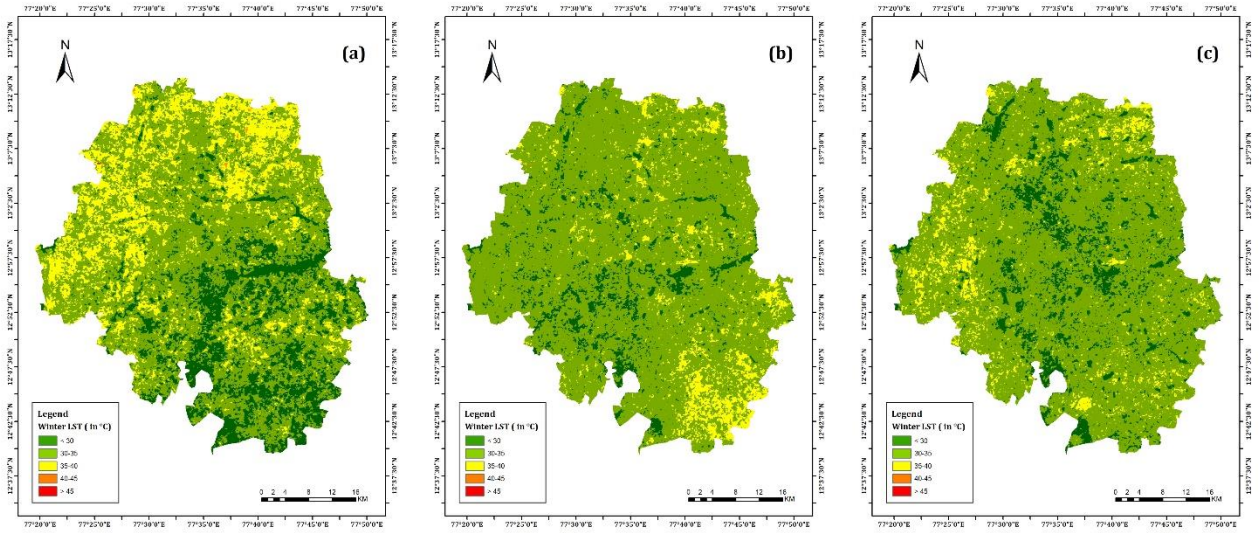

Figure 4 Winter LST distribution in the study area: (a) 2005, (b) 2015, and (c) 2025.

As the results show, summer LST patterns had intensified sharply in summer 2015. The area under <30°C declined by 345.46 sq. km, reducing its spatial extent to just 56.49 sq. km. Simultaneously, the 35-40°C class expanded substantially to 719.66 sq. km, representing an increase of 335.15 sq. km (87.16%) over the decade. More critically, high- and extreme-temperature zones emerged more prominently. The 40-45°C category increased to 5.01 sq. km, while areas exceeding 45°C, though spatially limited, were clearly detectable. These changes indicate rapid surface warming driven by accelerated land-use conversion, loss of vegetative cover, and increased heat retention by built-up materials.

In 2025, the summer thermal structure exhibited a partial redistribution rather than continued escalation. The <30°C class recovered to 174.81 sq. km. This suggests some improvement in localized cooling conditions. The 30-35°C category expanded further, reaching 1,795.00 sq. km and becoming the most dominant thermal class across the city. In contrast, the 35-40°C class contracted sharply to 225.57 sq. km, and extreme heat categories declined only slightly, with areas above 45°C

reducing to just 0.03 sq. km. This shift suggests a stabilization of surface temperatures into moderately high ranges rather than unchecked progression toward extreme heat, potentially reflecting dispersed greening efforts, evolving building materials, or a more uniform urban thermal response as the city matured structurally.

The observed reduction in extreme temperature classes should not be interpreted as an overall improvement in thermal conditions; rather, it reflects a redistribution of thermal intensity across the urban landscape. The expansion of the 30-35°C class, along with the contraction of higher-temperature ranges, indicates a process of thermal homogenization in which heat becomes more evenly distributed rather than concentrated in localized hotspots. This pattern is closely linked to the spatial expansion of built-up areas, which enhances the overall heat-retention capacity of the urban system while reducing sharp thermal gradients. In rapidly urbanizing environments, replacing heterogeneous land cover with more uniform impervious surfaces results in a more consistent but elevated thermal baseline. Therefore, the decline in extreme heat categories does not signify mitigation of urban heat stress, but rather a shift toward widespread moderate thermal conditions. This transition must be interpreted in the context of spatial distribution and urban structure rather than as an absolute reduction in thermal intensity. The increase in land surface temperature is strongly associated with the expansion of built-up areas and the decline in vegetation cover, as impervious materials reduce evapotranspiration and increase heat storage. At the same time, the loss of water bodies further limits local cooling effects and intensifies thermal stress. These findings align with previous studies that report a positive relationship between built-up density and LST and a negative relationship between vegetation indices and surface temperature [47, 48]. Overall, the spatial redistribution of temperature classes demonstrates that urban growth not only elevates thermal intensity but also fundamentally alters the spatial structure of heat distribution across the city.

Winter season LST patterns follow a similar but more subdued trajectory. In 2005, winter temperatures below 30°C covered 404.43 sq. km, while temperatures in the 30-35°C range covered 1,333.40 sq. km. Moderately warm surfaces in the 35-40°C range extended across 454.99 sq. km, and temperatures above 40°C were negligible. A marked reduction in cooler surfaces was observed, with the <30°C class declining by 220.09 sq. km to 184.34 sq. km. in the year 2015, and at the same time, the 30-35°C category expanded substantially to 1,828.48 sq. km, indicating a general rise in background winter temperatures across the urban landscape. In 2025, winter conditions showed relative stabilization. The <30°C class declined marginally to 174.81 sq. km, while the 30-35°C category remained dominant at 1,795.00 sq. km. The 35-40°C class increased moderately to 225.57 sq. km, suggesting a gradual warming of winter surfaces. Although areas exceeding 40°C remained limited in extent, their persistent presence highlights increasing thermal inertia in dense built-up zones and reduced nocturnal cooling. Both the summer and winter seasons reveal a consistent pattern of thermal intensification between 2005 and 2015, followed by redistribution into moderately high-temperature ranges by 2025. The expansion of the 30-35°C class across seasons and the contraction of extreme temperature zones in recent years suggest that Bangalore's urban thermal environment is transitioning toward sustained moderate heat stress rather than episodic extremes. These trends align with observed urban heat island evolution in rapidly expanding Indian metropolitan regions. This underscores the growing importance of land-use planning, surface material choices, and urban greening strategies in moderating future thermal risks.

3.3 Seasonal Dynamics of UTFVI in Bangalore (2005-2025)

The Urban Thermal Field Variance Index (UTFVI) was employed to assess seasonal ecological thermal stress in Bangalore for 2005, 2015, and 2025 (Table 8; Figure 5 and Figure 6)**.** Extreme thermal stress was widespread, with the Strongest UTFVI category (>0.020) covering 930.15 sq. km. during the summer of 2005. Although areas under weak thermal stress (<0.005) occupied a considerable portion of the study area, the spatial distribution of higher UTFVI classes indicates localized thermal hotspots. This pattern reflects spatial heterogeneity in urban thermal conditions rather than uniform temperature distribution, consistent with findings from previous urban climate studies [44, 46]. The summer UTFVI patterns showed a clear redistribution of thermal stress in the year 2015. The Strongest category declined by 133.11 sq. km to 797.04 sq. km, while intermediate stress classes (Middle, Strong, and Stronger) expanded collectively by over 68 sq. km. The Weak category also increased to 1,167.76 sq. km. This change indicates that extreme thermal stress is fragmented into broader zones of moderate ecological degradation, consistent with rapid urban expansion and densification. The projected expansion of thermal stress zones underscores the need for climate-sensitive urban planning strategies. Increasing urban green spaces, preserving existing vegetation, and protecting water bodies can play a critical role in mitigating future heat stress. The adoption of sustainable urban design practices, such as reflective materials and improved urban ventilation, can help reduce heat accumulation. These findings highlight the importance of integrating thermal considerations into urban development policies to enhance long-term environmental sustainability and resilience.

Table 8 Summarized Table of UTFVI for Summer and Winter Seasons in 2005, 2015, 2025.

UTFVI	Area (in sq. km)			Net Change (in sq. km)			Change in Percentage		
	2005	2015	2025	2005-15	2015-25	2005-25	2005-15	2015-25	2005-25
Summer Season									
Weak	1103.47	1167.76	1122.88	+64.29	-44.88	+19.41	+5.83	-3.84	+1.76
Middle	53.57	77.79	80.82	+24.22	+3.03	+27.25	+45.21	+3.90	+50.87
Strong	54.03	77.48	81.60	+23.45	+4.12	+27.57	+43.40	+5.32	+51.03
Stronger	54.89	76.05	82.25	+21.16	+6.20	+27.36	+38.55	+8.15	+49.85
Strongest	930.15	797.04	828.57	-133.11	+31.53	-101.58	-14.31	+3.96	-10.92
Winter Season									
Weak	1075.48	1162.22	1149.77	+86.74	-12.45	+74.29	+8.07	-1.07	+6.91
Middle	50.62	83.88	73.36	+33.26	-10.52	+22.74	+65.71	-12.54	+44.92
Strong	51.92	84.65	73.81	+32.73	-10.84	+21.89	+63.04	-12.81	+42.16
Stronger	51.62	83.04	72.95	+31.42	-10.09	+21.33	+60.87	-12.15	+41.32
Strongest	966.48	782.33	826.22	-184.15	+43.89	-140.26	-19.05	+5.61	-14.51

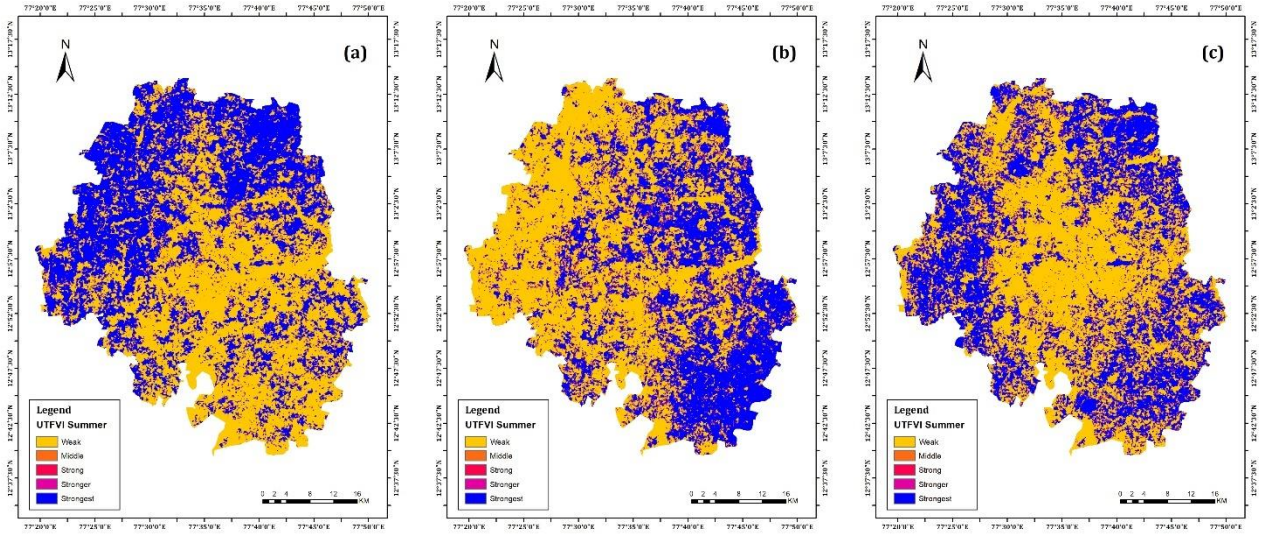

Figure 5 Summer UTFVI distribution in the study area: (a) 2005, (b) 2015, and (c) 2025.

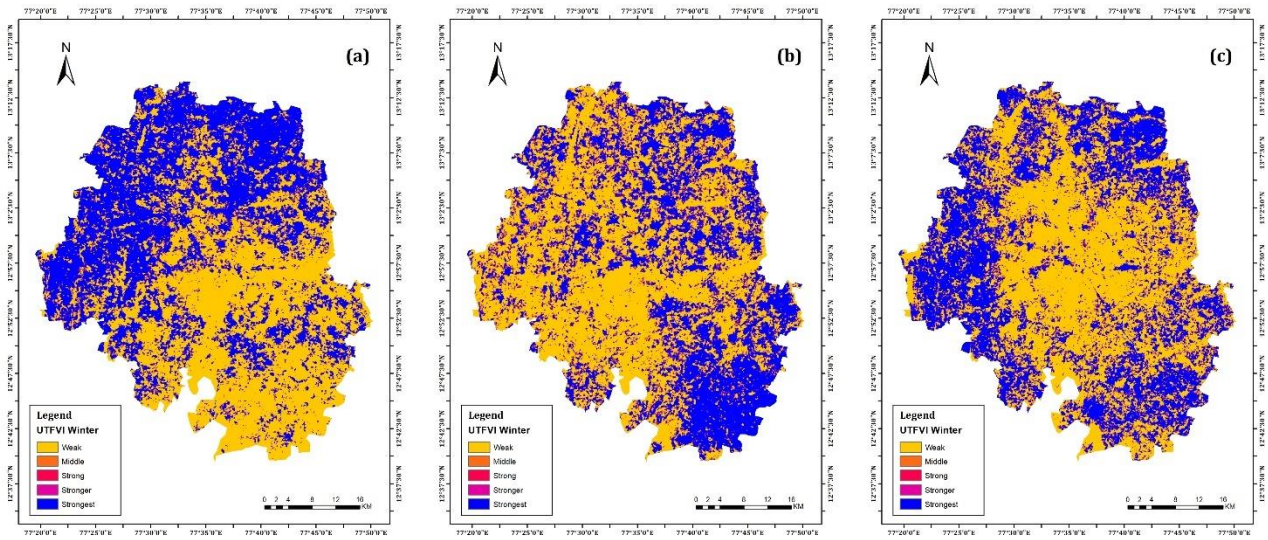

Figure 6 Winter UTFVI distribution in the study area: (a) 2005, (b) 2015, and (c) 2025.

In 2025, summer conditions stabilized further. Although the Strongest class increased slightly to 828.57 sq. km, it remained substantially lower than in 2005, reflecting a net reduction of 101.58 sq. km over two decades. Intermediate stress categories continued to expand, while the Weak category remained above its 2005 level. These patterns suggest persistent summer thermal stress, but with reduced dominance of the most ecologically degraded conditions. Winter UTFVI distributions indicate comparatively more stable ecological conditions. The Weak category expanded from 1,075.48 sq. km in 2005 to 1,162.22 sq. km in 2015 and remained dominant in 2025 (1,149.77 sq. km). In contrast, the Strongest category declined sharply from 966.48 sq. km in 2005 to 782.33 sq. km in 2015 and remained well below baseline levels in 2025. Over the full period, winter extreme stress areas decreased by 140.26 sq. km (14.51%). Overall, UTFVI trends in Bangalore reflect strong thermal intensification between 2005 and 2015, followed by partial stabilization and redistribution by 2025. Summer continues to exhibit higher ecological stress than winter. Still, the long-term

decline in the most extreme UTFVI classes suggests a gradual moderation of thermal degradation, which aligns closely with the observed seasonal LST dynamics.

3.4 Simulation of Future LULC for the Year 2045

3.4.1 Land Use and Land Cover Changes in Bangalore for the Predicted Year 2045

The projected LULC scenario for Bangalore in 2045, generated using the CA–ANN model, indicates the continuation of trends observed during the historical period (Figure 7). A comparison of LULC classes for 2020 and 2045 is presented in Table 9. Built-up land is projected to increase further from 501.89 sq. km in 2020 to 666.19 sq. km by 2045, an additional 164.30 sq. km. This growth highlights sustained urban expansion and densification, reflecting ongoing development pressures. Water bodies are projected to increase marginally from 18.43 sq. km to 19.81 sq. km. Although this change is minimal, it may indicate limited restoration efforts or natural recovery; however, the overall extent of surface water remains critically low. Dense vegetation is expected to decline substantially, decreasing from 484.37 sq. km to 373.25 sq. km, a loss of 111.17 sq. km. This reduction raises concerns about continued deforestation and fragmentation of green spaces. Cropland is also projected to decrease from 892.94 sq. km to 777.92 sq. km, suggesting conversion to urban land or degradation due to changing land management practices. Sparse vegetation is anticipated to decline slightly from 147.15 sq. km to 137.50 sq. km, indicating persistent pressure on remaining semi-natural landscapes. In contrast, barren land is projected to increase significantly from 153.32 sq. km in 2020 to 223.64 sq. km by 2045. This increase may reflect land degradation, soil exhaustion, or abandonment of marginal lands, emphasizing the need for land restoration and sustainable management strategies.

Table 9 Area coverage of different LULC classes in the years 2000, 2020, and 2045.

Class	2000	2020	2045
Built-Up Land	277.93 sq. km	501.89 sq. km	666.19 sq. km
Water Body	48.15 sq. km	18.43 sq. km	19.81 sq. km
Dense Vegetation	560.42 sq. km	484.37 sq. km	373.25 sq. km
Sparse Vegetation	622.37 sq. km	147.15 sq. km	137.50 sq. km
Crop Land	677.02 sq. km	892.94 sq. km	777.92 sq. km
Barren Land	12.23 sq. km	153.32 sq. km	223.64 sq. km

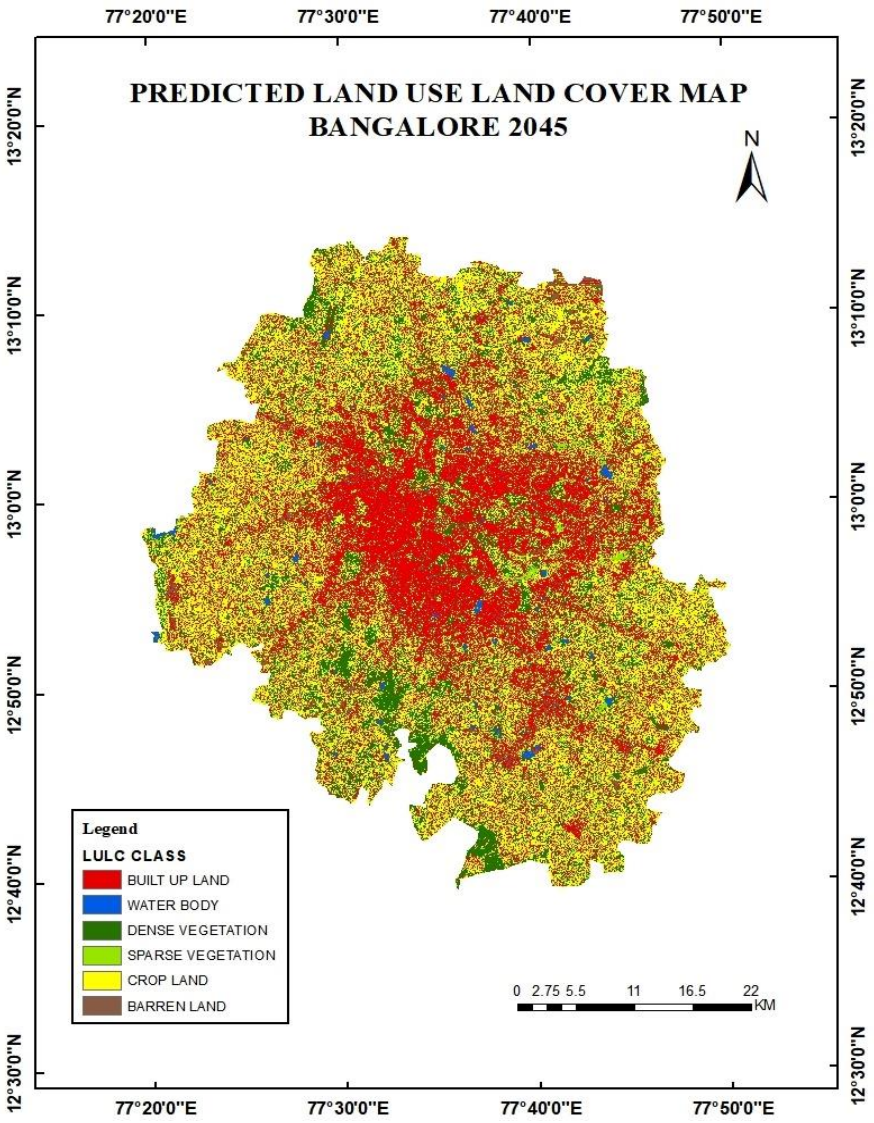

Figure 7 Predicted LULC Map of Bangalore for the year 2045.

3.4.2 Projected Land Surface Temperature Scenario for the Predicted Year 2045

Machine-learning-based projections indicate that Bangalore will continue to experience a gradual yet persistent rise in land-surface temperatures by 2045 (Table 10; Figure 8). The thermal landscape is expected to become increasingly dominated by moderately high summer temperatures. The 30-35°C class expands substantially, reaching 2,072.72 sq. km in 2045, representing a net increase of 665.42 sq. km from 2005 and 277.72 sq. km from 2025. This class emerges as the dominant summer temperature range, reflecting widespread surface warming associated with urban expansion.

Table 10 Changes in seasonal LST from 2005 to 2045 in the Summer and Winter seasons.

LST (in °C)	Area (in sq. km)				Net Change (sq. km)			Change in Percentage		
	2005	2015	2025	2045	2005-45	2015-45	2025-45	2005-45	2015-45	2025-45
Summer Season										
Less than 30	401.95	56.49	174.81	77.5	-324.45	21.01	-97.31	-80.72	37.19	-55.67
30-35	1407.3	1414.88	1795	2072.72	665.42	657.84	277.72	47.29	46.49	15.47
35-40	384.51	719.66	225.57	45.88	-338.63	-673.78	-179.69	-88.07	-93.64	-79.65
40-45	2.13	5.01	0.71	0	-2.13	-5.01	-0.71	-100.00	-100.00	-100.00
Above 45	0.23	0.07	0.03	0	-0.23	-0.07	-0.03	-100.00	-100.00	-100.00
Winter Season										
Less than 30	404.43	184.34	174.81	86.66	-317.77	-97.68	-88.15	-78.57	-52.99	-50.42
30-35	1333.4	1828.48	1795	2064.93	731.53	236.45	269.93	54.88	12.93	15.04
35-40	454.99	182.58	225.57	44.51	-410.48	-138.07	-181.06	-90.22	-75.63	-80.23
40-45	3.07	0.68	0.71	0	-3.07	-0.68	-0.71	-100.00	-100.00	-100.00
Above 45	0.23	0.03	0.03	0	-0.23	-0.03	-0.03	-100.00	-100.00	-100.00

The cooler zones below 30°C decline sharply over the long-term results, shrinking from 401.95 sq. km in 2005 to 77.50 sq. km in the projected year 2045. This indicates a significant loss of thermally moderated surfaces, such as dense vegetation and water bodies. Higher temperature classes show a notable redistribution rather than escalation. The 35-40°C class contracts dramatically, from 384.51 sq. km in 2005 to just 45.88 sq. km in 2045, while temperatures exceeding 40°C are projected to disappear entirely. This suggests that extreme summer heat becomes spatially less extensive and is replaced by widespread moderately high temperatures.

The results reveal a similar warming tendency in the simulated winter projections. The 30-35°C class expands markedly from 1,333.40 sq. km in 2005 to 2,064.93 sq. km in 2045, indicating rising baseline temperatures even during cooler months. At the same time, the areas within the 35-40°C class decline sharply, and all temperature categories above 40°C vanish by 2045. The persistence of warmer winter conditions reflects increased thermal inertia driven by dense built-up areas and reduced seasonal cooling capacity. The projected LST patterns for Bangalore suggest a transition toward a thermally homogenized urban surface, with moderate-to-high temperatures across the seasons. The extreme heat is becoming less spatially concentrated but more structurally widespread.

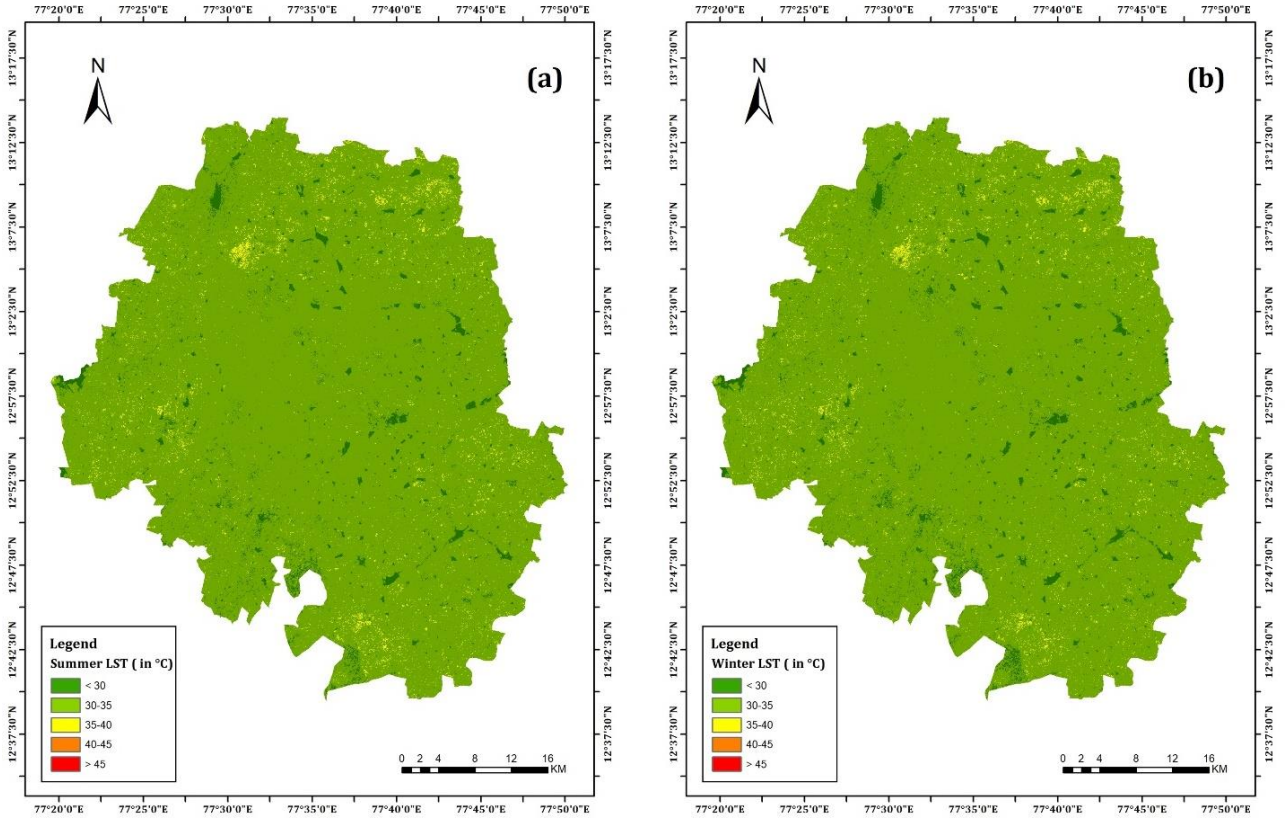

Figure 8 Simulated Maps of (a) summer and (b) winter LST distribution for the year 2045 in the study area.

3.4.3 Projected UTFVI Scenario for the Predicted Year 2045

Projected UTFVI patterns for 2045 underscore the ecological consequences of Bangalore's changing thermal environment (Table 11; Figure 9). In summer, areas within the Weak ecological stress category remain relatively stable, with a marginal change from 1,103.47 sq. km in 2005 to 1,110.43 sq. km in 2045. This apparent stability, however, conceals a significant expansion of mid-

level stress categories. The Middle, Strong, and Stronger classes more than double in spatial extent, collectively increasing by over 200 sq. km compared to 2005. Concurrently, the Strongest UTFVI category declines from 930.15 sq. km in 2005 to 720.87 sq. km in 2045, which shows a net reduction of 209.28 sq. km. This reduction does not indicate ecological recovery but rather a redistribution of thermal stress from extreme hotspots to broader zones of moderate degradation. Thermal stress becomes more spatially diffuse, affecting a larger portion of the urban landscape. Winter UTFVI projections reveal similar trends. Although the Weak category decreases slightly from its 2015 peak, intermediate stress categories expand substantially. The Middle, Strong, and Stronger classes together increase by more than 190 sq. km between 2005 and 2045. In contrast, the Strongest category contracts by 230.40 sq. km during the same period, which reinforces the trend of declining extreme stress but increasing moderate ecological vulnerability.

Table 11 Seasonal changes in UTFVI from 2005 to 2045 for the Summer and the Winter seasons in the study area.

UTFVI	Area (in sq. km)				Net Change (sq. km)			Change in Percentage		
	2005	2015	2025	2045	2005-45	2015-45	2025-45	2005-45	2015-45	2025-45
Summer										
Weak	1103.47	1167.76	1122.88	1110.43	6.96	-57.33	-12.45	0.63	-4.91	-1.11
Middle	53.57	77.79	80.82	123.61	70.04	45.82	42.79	130.75	58.9	52.94
Strong	54.03	77.48	81.6	122.65	68.62	45.17	41.05	126.99	58.3	50.31
Stronger	54.89	76.05	82.25	118.53	63.64	42.48	36.28	115.95	55.86	44.11
Strongest	930.15	797.04	828.57	720.87	-209.28	-76.17	-107.70	-22.50	-9.56	-13.00
Winter										
Weak	1075.48	1162.22	1149.77	1100.07	24.59	-62.15	-49.70	2.29	-5.35	-4.32
Middle	50.62	83.88	73.36	121.61	70.99	37.73	48.25	140.27	44.98	65.76
Strong	51.92	84.65	73.81	121.19	69.27	36.54	47.38	133.43	43.17	64.2
Stronger	51.62	83.04	72.95	117.16	65.54	34.12	44.21	126.97	41.09	60.63
Strongest	966.48	782.33	826.22	736.08	-230.40	-46.25	-90.14	-23.84	-5.91	-10.91

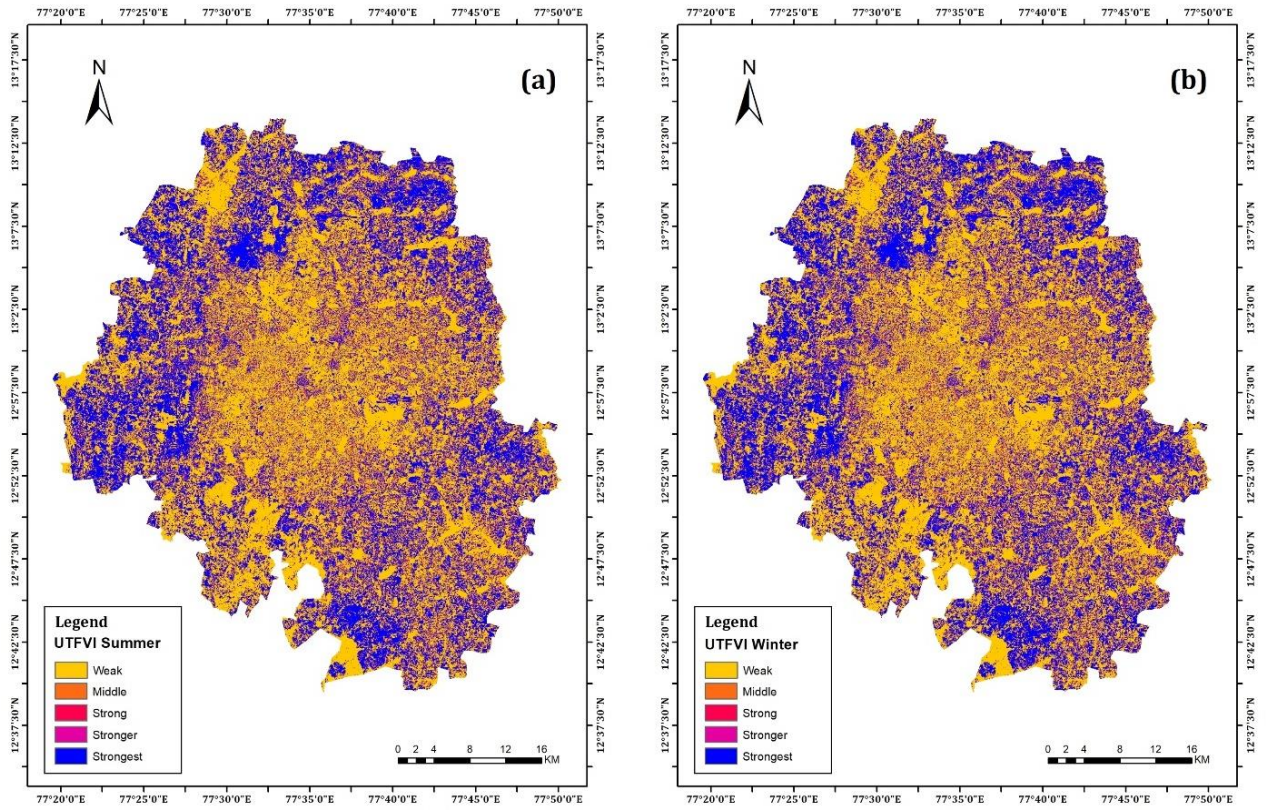

Figure 9 Simulated (a) summer and (b) winter LST distribution for the year 2045 in the study area.

The UTFVI projections indicate that Bangalore's future thermal environment will be characterized less by isolated extreme stress zones and more by widespread ecological strain. The combined LST and UTFVI trajectories confirm that continued urbanization and increasing density, along with declining vegetative cover, are reshaping the city's future. The thermal structure, transforming heat stress from a localized phenomenon into an unescapable urban condition in the future.

4. Conclusion

The outcomes of this study show that Bangalore's thermal environment has experienced significant changes driven by persistent changes in land use and land cover over the past 20 years. The growth of built-up land increased from 277.93 sq. km (12.64%) in 2000 to 501.89 sq. km (22.83%) in 2020, and is expected to reach 666.19 sq. km (30.30%) by 2045, marking the major spatial change in Bangalore's urban landscape. The vegetation and water bodies, which serve as the city's natural cooling systems, were significantly affected by this expansion. The water bodies declined by 60% during the study period, 2000-2020. The combined losses of dense and sparse vegetation exceeded 660 sq. km, indicating a significant decline in the city's environmental capacity. The observed patterns of urban land surface temperature closely reflect these changes in land cover. According to the seasonal LST analysis, the surface warming has been clearly intensified, especially in the summer. While the data shows we are seeing those extreme 45°C spikes again, the baseline temperature is rising. Even the winter conditions offer less relief in the city these days. The urban land becomes dense concrete that traps the day's heat like a battery, creating thermal inertia that

keeps the thermometer rising long after the sun goes down. The pattern is clear. We are no longer dealing with isolated heat pockets. We are shifting toward a world that is constantly warmer. The ecological data backs this up, though you have to look closely to see it. The Urban Thermal Field Variance Index (UTFVI) shows that the most severe red zones have actually shrunk slightly on the city's surface since 2005. The medium-stress zones are spreading like an infection across the city's map. By 2045, the areas labeled Bad and Worse will no longer be outliers; they will be the practical norm. The cause is simple physics. We have traded vegetation and water for impervious pavement. As the concrete spreads, so does the heat. If we don't change how we build, especially in the fast-growing peri-urban fringes, this trajectory is locked in. We cannot engineer our way out of this with better air conditioning alone. We need integrated planning that respects the climate. That means protecting the few remaining green spaces, restoring water bodies, and designing a city that can actually breathe. This current study is not just a projection. It is a warning that we need to stop building heat traps and start building a livable future.

Acknowledgments

The availability of open-access geospatial datasets from the Survey of India, the National Aeronautics and Space Administration (NASA), the United States Geological Survey (USGS), the Indian Space Research Organization (ISRO), and Google Earth was essential for this research.

Author Contributions

The author was involved in all stages of the research process, including conceptualization, methodological design, data curation, software implementation, validation, analysis, and drafting of the original manuscript. Additionally, the author reviewed and edited the final version.

Competing Interests

The author has declared that no competing interests exist.

Data Availability Statement

The data for this study come from publicly available sources. We obtained satellite imagery from the United States Geological Survey Landsat archive and processed it with Google Earth Engine. We accessed additional spatial datasets from open-source geospatial repositories. All data supporting this study's findings are available on the relevant public platforms.

AI-Assisted Technologies Statement

The Grammarly tool was used solely for language editing to improve grammar, clarity, and readability during manuscript preparation. The Grammarly tool did not contribute to the generation of scientific content, data analysis, interpretation, or conclusions. All the components of the manuscript, including research design, data collection, methodology, analysis and writing, were prepared independently by the author. The author has carefully reviewed and verified all contents and takes full responsibility for the accuracy, originality, and integrity of the manuscript.

References

1. Foley JA, DeFries R, Asner GP, Barford C, Bonan G, Carpenter SR et al. Global consequences of land use. Science. 2005; 309: 570-574.
2. Ellis EC, Ramankutty N. Putting people in the map: Anthropogenic biomes of the world. Front Ecol Environ. 2008; 6: 439-447.
3. Bürgi M, Hersperger AM, Schneeberger N. Driving forces of landscape change-current and new directions. Landsc Ecol. 2005; 19: 857-868.
4. Angel S, Parent J, Civco DL, Blei A, Potere D. The dimensions of global urban expansion: Estimates and projections for all countries, 2000-2050. Prog Plan. 2011; 75: 53-107.
5. Seto KC, Fragkias M, Güneralp B, Reilly MK. A meta-analysis of global urban land expansion. PloS One. 2011; 6: e23777.
6. Batty M. The size, scale, and shape of cities. Science. 2008; 319: 769-771.
7. Herold M, Goldstein NC, Clarke KC. The spatiotemporal form of urban growth: Measurement, analysis and modeling. Remote Sens Environ. 2003; 86: 286-302.
8. IPBES Secretariat. Global assessment report on biodiversity and ecosystem services of the Intergovernmental Science-Policy Platform on Biodiversity and Ecosystem Services [Internet]. Bonn, Germany: IPBES secretariat; 2019. Available from: https://files.ipbes.net/ipbes-web-prod-public-files/inline/files/ipbes_global_assessment_report_summary_for_policymakers.pdf.
9. Brauer M, Amann M, Burnett RT, Cohen A, Dentener F, Ezzati M, et al. Exposure assessment for estimation of the global burden of disease attributable to outdoor air pollution. Environ Sci Technol. 2012; 46: 652-660.
10. McDonald RI, Colbert ML, Hamann M, Simkin R, Walsh B. Nature in the urban century: A global assessment of where and how to conserve nature for biodiversity and human wellbeing [Internet]. Arlington, VA: The Nature Conservancy; 2018. Available from: https://www.nature.org/content/dam/tnc/nature/en/documents/TNC_NatureintheUrbanCentury_FullReport.pdf.
11. United Nations-Department of Economic and Social Affairs. World Urbanization Prospects: 2018 Revision [Internet]. New York, NY: United Nations; 2019. Available from: https://population.un.org/wup/assets/WUP2018-Report.pdf.
12. Jensen JR. Remote sensing of the environment: An earth resource perspective. 2nd ed. Pearson Prentice Hall; 2007.
13. Lu D, Weng Q. A survey of image classification methods and techniques for improving classification performance. Int J Remote Sens. 2007; 28: 823-870.
14. Belgiu M, Drăguţ L. Random forest in remote sensing: A review of applications and future directions. ISPRS J Photogramm Remote Sens. 2016; 114: 24-31.
15. Zhu Z, Woodcock CE. Continuous change detection and classification of land cover using all available Landsat data. Remote Sens Environ. 2014; 144: 152-171.
16. Roy DP, Wulder MA, Loveland TR, Ce W, Allen RG, Anderson MC, et al. Landsat-8: Science and product vision for terrestrial global change research. Remote Sens Environ. 2014; 145: 154-172.
17. Chander G, Markham BL, Helder DL. Summary of current radiometric calibration coefficients for Landsat MSS, TM, ETM+, and EO-1 ALI sensors. Remote Sens Environ. 2009; 113: 893-903.

18. Vermote E, Justice C, Claverie M, Franch B. Preliminary analysis of the performance of the Landsat 8/OLI land surface reflectance product. Remote Sens Environ. 2016; 185: 46-56.
19. Foga S, Scaramuzza PL, Guo S, Zhu Z, Dilley Jr RD, Beckmann T, et al. Cloud detection algorithm comparison and validation for operational Landsat data products. Remote Sens Environ. 2017; 194: 379-390.
20. Carlson TN, Gillies RR, Perry EM. A method to make use of thermal infrared temperature and NDVI measurements to infer surface soil water content and fractional vegetation cover. Remote Sens Rev. 1994; 9: 161-173.
21. Zha Y, Gao J, Ni S. Use of normalized difference built-up index in automatically mapping urban areas from TM imagery. Int J Remote Sens. 2003; 24: 583-594.
22. Oke TR. The energetic basis of the urban heat island. Q J R Meteorol Soc. 1982; 108: 1-24.
23. Voogt JA, Oke TR. Thermal remote sensing of urban climates. Remote Sens Environ. 2003; 86: 370-384.
24. Qin Z, Karnieli A, Berliner P. A mono-window algorithm for retrieving land surface temperature from Landsat TM data and its application to the Israel-Egypt border region. Int J Remote Sens. 2001; 22: 3719-3746.
25. Sobrino JA, Jiménez-Muñoz JC, Paolini L. Land surface temperature retrieval from LANDSAT TM 5. Remote Sens Environ. 2004; 90: 434-440.
26. Chen XL, Zhao HM, Li PX, Yin ZY. Remote sensing image-based analysis of the relationship between urban heat island and land use/cover changes. Remote Sens Environ. 2006; 104: 133-146.
27. Tomlinson CJ, Chapman L, Thornes JE, Baker C. Remote sensing land surface temperature for meteorology and climatology: A review. Meteorol Appl. 2011; 18: 296-306.
28. Rasul A, Balzter H, Smith C. Diurnal and seasonal variation of surface urban cool and heat islands in the semi-arid city of Erbil, Iraq. Climate. 2016; 4: 42.
29. Gunawardena KR, Wells MJ, Kershaw T. Utilising green and bluespace to mitigate urban heat island intensity. Sci Total Environ. 2017; 584: 1040-1055.
30. Rahmani N, Sharifi A. Comparative analysis of the Surface Urban Heat Island (SUHI) effect based on the Local Climate Zone (LCZ) classification scheme for two Japanese cities, Hiroshima, and Sapporo. Climate. 2023; 11: 142.
31. Estoque RC, Murayama Y, Myint SW. Effects of landscape composition and pattern on land surface temperature: An urban heat island study in the megacities of Southeast Asia. Sci Total Environ. 2017; 577: 349-359.
32. Gupta RK. Identifying urban hotspots and cold spots in Delhi using the Biophysical Landscape framework. Ecol Econ Soc. 2024; 7: 137-155.
33. Hassan T, Zhang J, Prodhan FA, Pangali Sharma TP, Bashir B. Surface urban heat islands dynamics in response to LULC and vegetation across South Asia (2000-2019). Remote Sens. 2021; 13: 3177.
34. Kikon N, Singh P, Singh SK, Vyas A. Assessment of urban heat islands (UHI) of Noida City, India using multi-temporal satellite data. Sustain Cities Soc. 2016; 22: 19-28.
35. Wang H, Zhang Y, Tsou JY, Li Y. Surface urban heat island analysis of Shanghai (China) based on the change of land use and land cover. Sustainability. 2017; 9: 1538.

36. Muhammad R, Zhang W, Abbas Z, Guo F, Gwiazdzinski L. Spatiotemporal change analysis and prediction of future land use and land cover changes using QGIS MOLUSCE plugin and remote sensing big data: A case study of Linyi, China. Land. 2022; 11: 419.
37. Uddin MS, Mahalder B, Mahalder D. Assessment of land use land cover changes and future predictions using CA–ANN simulation for Gazipur City Corporation, Bangladesh. Sustainability. 2023; 15: 12329.
38. Subedi P, Subedi K, Thapa B. Application of a hybrid cellular automaton-Markov (CA-Markov) model in land-use change prediction: A case study of Saddle Creek Drainage Basin, Florida. Appl Ecol Environ Sci. 2013; 1: 126-132.
39. Gupta R. GIS-based analysis of land surface characteristics and urban heat islands in metropolitan cities of India. Int J Eng Geosci. 2025; 10: 440-455.
40. Gharaibeh A, Shaamala A, Obeidat R, Al-Kofahi S. Improving land-use change modeling by integrating ANN with Cellular Automata-Markov Chain model. Heliyon. 2020; 6: e05092.
41. Gündüz Hİ. Land-use land-cover dynamics and future projections using GEE, ML, and QGIS-MOLUSCE: A case study in Manisa. Sustainability. 2025; 17: 1363.
42. Nagne AD, Vibhute AD, Dhumal RK, Kale KV, Mehrotra SC. Urban LULC change detection and mapping spatial variations of Aurangabad city using IRS LISS-III temporal datasets and supervised classification approach. In: Data Analytics and Learning: Proceedings of DAL 2018. Singapore: Springer Singapore; 2018. pp. 369-386.
43. Ward K, Lauf S, Kleinschmit B, Endlicher W. Heat waves and urban heat islands in Europe: A review of relevant drivers. Sci Total Environ. 2016; 569: 527-539.
44. Yuan F, Bauer ME. Comparison of impervious surface area and normalized difference vegetation index as indicators of surface urban heat island effects in Landsat imagery. Remote Sens Environ. 2007; 106: 375-386.
45. Liu L, Zhang Y. Urban heat island analysis using the Landsat TM data and ASTER data: A case study in Hong Kong. Remote Sens. 2011; 3: 1535-1552.
46. Zhou D, Xiao J, Bonafoni S, Berger C, Deilami K, Zhou Y, et al. Satellite remote sensing of surface urban heat islands: Progress, challenges, and perspectives. Remote Sens. 2018; 11: 48.
47. Weng Q, Lu D, Schubring J. Estimation of land surface temperature-vegetation abundance relationship for urban heat island studies. Remote Sens Environ. 2004; 89: 467-483.
48. Zhou D, Zhao S, Liu S, Zhang L, Zhu C. Surface urban heat island in China's 32 major cities: Spatial patterns and drivers. Remote Sens Environ. 2014; 152: 51-61.